Morphology and Molecular Mobility of Several Kinds of Polyethylene Specimens by ^{13}C Solid-State NMR and X-ray Diffraction Techniques

Yoshimi Shimizu,† Yuko Harashina,‡ Yuri Sugiura, and Masaru Matsuo*

Department of Textile and Apparel Science, Faculty of Human Life and Environment, Nara Women's University, Nara 630, Japan

Received November 29, 1994; Revised Manuscript Received April 17, 1995®

ABSTRACT: The morphology and molecular mobility of polyethylene were investigated by X-ray diffraction and ^{13}C solid-state NMR as a function of temperature. The test specimens chosen are melt films, single-crystal mats, undrawn dry gel films, and ultradrawn films with a draw ratio of 300. The semilogarithmic plot of the ^{13}C magnetization of the peak height of the line at 33 ppm indicated the existence of three different kinds of spin–lattice relaxation time (T_{1C}): a slow decay time, an intermediate decay time, and a rapid decay time for the orthorhombic crystal form. Among the test specimens, the decay time of the ultradrawn gel film was the longest. The spin–spin relaxation time (T_{2C}) indicated that the noncrystalline component consists of an interfacial region and a rubber-like amorphous region with extensive molecular mobility. For single-crystal mats and dry gel films, the lenght of the interfacial region calculated using both the mass fraction of the interfacial region by ^{13}C NMR and the long period by X-ray scattering was almost equal to the length of the interfacial region estimated by analyzing a systematic deviation of the X-ray scattering curves at large angle tail from Porod's law. Furthermore, the crystallinity at room temperature estimated by ^{13}C NMR was also in good agreement with the results by density and X-ray diffraction. With increasing temperature, T_{1C} for the crystalline region became shorter, while T_{2C} for the noncrystalline region became longer, indicating more active molecular mobility. The crystallinity estimated by ^{13}C NMR was confirmed to decreased with increasing temperature. This tendency was in good agreement with the results obtained by X-ray diffraction using Ruland's method.

Introduction

In recent years, research on the preparation of fibers and films with high modulus and high strength has become a topic of increasing interest.[1–10] This research is based on the assumption that the theoretical Young's modulus and tensile strength of polymeric materials could be realized if the chains were fully aligned and extended and if the specimens were almost completely crystalline. Interesting results have been obtained for polyethylene.[1–8] According to recent studies by Matsuo et al., the Young's modulus of ultradrawn polyethylene films of 20 °C reached 216 GPa. This value is nearly equal to the crystal lattice modulus of polyethylene.[8]

The deformation mechanism of polyethylene gel films and single-crystal mats up to a draw ratio of 300 has been discussed in terms of morphological aspects as studied by wide-angle X-ray diffraction (WAXD), small-angle X-ray scattering (SAXS), small-angle light scattering (SALS), and scanning electron micrographs (SEM).[5–8] Through a series of experimental results, the morphology of the dry gel films was found to be similar to that of single-crystal mats, and the facile drawability was thought to be due to the transformation from folded to fibrous crystals.

Apart from the above static information, the morphology of polyethylene has been investigated in terms of dynamic information such as molecular mobility using high-resolution solid-state ^{13}C NMR by Ando et al.[11,12] and VanderHart et al.[13,14] Their spectra showed one main peak at 33 ppm for single-crystal mats and a small shoulder in addition to the main peak for melt-crystallized films and drawn films, indicating the existence of two kinds of carbons with different magnetic environments. These evaluations have been done in terms of chemical shifts and spin–lattice and spin–spin relaxation times. Based on a series of ^{13}C NMR studies, the 33 ppm peak corresponds to the average of the principal values of the chemical shift tensor for trans–trans methylene sequences of polyethylene or *n*-paraffins in orthorhombic crystal form,[15–17] while the 31 ppm value is close to that observed for polyethylene in solution.[17] Thus, these lines were assigned to the crystalline and the noncrystalline components, respectively. This assignment was confirmed in terms of the difference between spin–lattice relaxation times by VanderHart et al.[13] They reported that crystallinity can be estimated from the peak intensities of the two lines under the cross-polarization condition, and the value is in good agreement with that measured by the density method. Furthermore, VanderHart and Perez proposed a ^{13}C NMR method for determining the partitioning of end group and side branches between the crystalline and noncrystalline regions in polyethylene.[18] They pointed out that from the pure crystalline and noncrystalline regions and from an independent knowledge of defect concentrations, the partitioning of each defect between the crystalline and noncrystalline regions may be deduced and ethyl branches exist in the crystals but the concentration is much lower than that in the noncrystalline region. Another estimation was done by Kitamaru et al. for the noncrystalline component.[19] They pointed out that the noncrystalline component can be classified into two regions: a rubber-like amorphous component and an interfacial noncrystalline one.

Apart from the detailed studies of polyethylene in terms of dynamic aspects, there have been few reports comparing information obtained from X-ray diffraction and high-resolution solid-state ^{13}C NMR.[20] That is, it is of interest to study whether the results for interfacial length and crystallinity obtained by X-ray diffraction

† Present address: Shouwa Electric Co. Ltd.
‡ Present address: Toray Co. Ltd.
* To whom all correspondence should be addressed.
® Abstract published in *Advance ACS Abstracts,* August 15, 1995.

0024-9297/95/2228-6889$09.00/0

are in good agreement with those obtained by ^{13}C NMR. One purpose for this study is that it will help to elucidate the important relationship between morphology and molecular dynamics, which is one of the essential characteristics of crystalline polymers. We are also interested in confirming the decrease in crystallinity with increasing temperature by ^{1}H DD/MAS ^{13}C NMR, although this tendency was already reported by X-ray diffraction. If this is the case, the decrease in the Young's modulus of crystalline polymers with temperature is thought to be due to the decrease in crystallinity, as discussed in the previous work.[21]

Based on this concept, this paper deals with the morphology of dried gel films, single-crystal mats, and ultrahigh molecular weight polyethylene (UHMWPE) by high-resolution solid-state ^{13}C NMR, and the results obtained are mainly discussed in comparison with X-ray diffraction data. The ^{13}C NMR measurements are carried out in a manner similar to the method of Horii et al.[19,22,23]

Experimental Section

Sample Preparation. (1) Single-Crystal Mats. The sample used in this experiment was linear polyethylene with a molecular weight of 3×10^6 (Hizex Million 240M). The solvent was *p*-xylene. A *p*-xylene solution with a concentration of 0.01 g/100 mL was prepared by heating the well-blended polymer/solvent mixture at 135 °C for 40 min under nitrogen. The solution was cooled slowly to 85 °C and kept for 20 h to improve thermal crystallization. After that, the solution was cooled slowly to room temperature. As described in a previous paper,[24] a lot of ethanol was then introduced into the *p*-xylene solution, and the solution was stirred for 24 h at room temperature. The mixed solvent was decanted and new ethanol was introduced again. The treatment was repeated five times to remove *p*-xylene fully from the single-crystal mats by ethanol substitution. The single crystals were separated as a residue after pouring the solution onto a glass filter. The single crystals in a wet state were scattered on a glass plate to avoid bonding between single crystals during solvent evaporation under ambient conditions. The single crystals were vacuum-dried for 1 day at room temperature to remove residual traces of solvent and were then pressed at 20 or 5 MPa. The former and latter specimens are termed SC20 and SC5, respectively. The single-crystal mats were brittle.

(2) Gel Films. The samples were prepared by the method proposed by Smith and Lemstra,[1] using linear polyethylene with a viscosity-average molecular weight of 6×10^6. The gel films were stretched up to 300 times at 135 °C under nitrogen. Some of the dried gel films were annealed at 130 °C for 1 h and cooled slowly to room temperature to improve crystallinity as much as possible. Such annealed specimens were prepared to analyze the temperature dependence of crystallinity on the basis of ^{13}C NMR spectra and X-ray diffraction intensity.

(3) Melt Films. Crude pellets of low molecular weight polyethylene (LMWPE) with a molecular weight of 4×10^4 (Sumikathen G201) were treated with ethanol for 30 h in a Soxhlet extractor before their use as specimens. The extracted pellets were sandwiched between Teflon sheets at 245 °C for 15 min at a pressure of 14 MPa. The molten samples were quenched in an ice water bath to prepare amorphous specimens. These specimens were prepared to study the spin–lattice and spin–spin relaxation times of the noncrystalline region.

Some gel and melt films were annealed at 130 °C for 1 h and cooled to room temperature very slowly. This treatment was done to improve the crystallinity as much as possible in order to study the temperature dependence of crystallinity.

Sample Characterization. The X-ray measurements were carried out with a 12-kW rotating-anode X-ray generator (Rigaku RDA-rA operated at 200 mA and 40 kV). The WAXD measurement was carried out with point focusing using a system in which the incident beam was collimated by a collimator 2 mm in diameter, and the diffraction beam was measured by a square slit of 0.9 mm × 0.9 mm. The intensity distribution was measured at a step interval of 0.1° with a time interval of 40 s in the desired range of twice the Bragg angle. SAXS intensity distributions were detected with a position-sensitive proportional counter (PSPC). These measurements have been described elsewhere.[7,8]

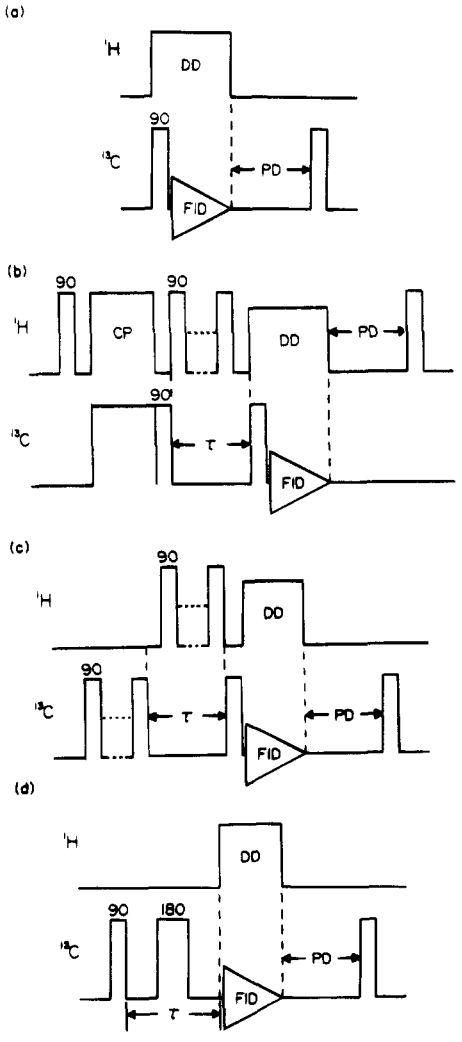

Figure 1. Pulse sequences used in this paper: (a) DD/MAS ^{13}C NMR without CP; (b) pulse sequence with CP developed by Torchia; (c) pulse sequence measured by the standard saturation–recovery pulse sequence without CP; (d) pulse sequence by the standard saturation–recovery pulse sequence without ^{1}H decoupling for a given time interval τ.

^{1}H DD/MAS ^{13}C NMR measurements were carried out at room temperature with a JEOL JM-EX270 spectrometer operating at a field of 6.35 T. A radio frequency of 67.5 MHz was used for detection of ^{13}C resonance. MAS was carried out at a rate of 4.5 kHz with a cylinder-type rotor made of zirconia and poly(amide imide) resins. The chemical shifts relative to tetramethylsilane (Me_4Si) were determined from the CH line (29.5 ppm) of solid adamantane as an external reference.

The pulse sequences used are schematically shown in Figure 1. Pulse sequence a is used to obtain ^{13}C spectra without cross-polymerization (CP). If the waiting time PD after the acquisition of FID is approximately set, one can obtain the spectrum containing partial or total contributions from the components in the structure. Pulse sequence b with CP developed by Torchia[25] was used to measure spin–lattice relaxation times (T_{1C}) longer than several tens of seconds. The spin–lattice relaxation times T_{1H} of the ^{1}H magnetization were also obtained by the pulse sequence [$^{H}(180°-\tau-90°)-CP-^{C}(FID)$], where one measures the magnetization that appears through the CP process after relaxation of the ^{1}H magnetization during the time τ. Spin–lattice relaxation times shorter than a few seconds were measured by the standard saturation–recovery pulse sequence c without CP. Pulse sequence d was used to

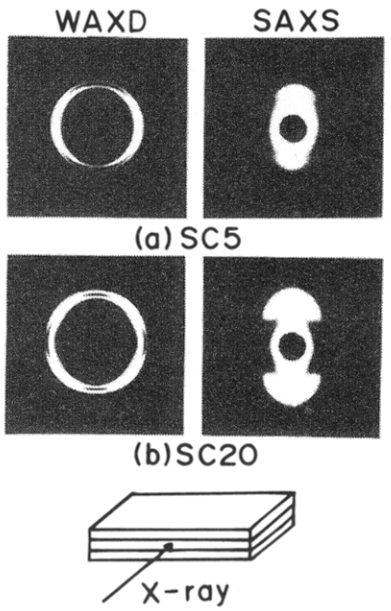

Figure 2. WAXD and SAXS patterns (end view) of single-crystal mats SC5 and SC20.

estimate the ^{13}C spin–spin relaxation by measuring FID under the DD condition after relaxing the transverse magnetization without ^{1}H decoupling for a given time interval τ. It is possible to estimate longer T_2 values in the absence of the contributions from a rigid or less mobile component by a proper choice of τ.

Results and Discussion

Figure 2 shows WAXD and SAXS patterns of SC5 and SC20. The WAXD and SAXS patterns of SC5 together indicate that the specimens are composed of single-crystal mats that are highly oriented with their large flat faces parallel to the film surface; the c-axes were oriented perpendicular to the large flat faces. These profiles resemble those observed in dried gel films. By contrast, the WAXD pattern of SC20, which was pressed at 20 MPa, exhibits four diffraction arcs from the (200) plane in spite of the SAXS pattern showing the scattering maxima in the meridional direction. Both patterns indicate that the a-axes are tilted at about 40° away from the surface normal of the mat face. The diffraction peak of the (020) plane in the horizontal direction was confirmed by a diffractometer. Judging from these diffraction arcs, the tilting is probably caused by slipping between crystals on the crystal b–c plane as a result of shear induced by the compressive stress during the sample preparation. This indicates that the c-axes are tilted at about 50° from the surface normal of the mat face.[22]

Figure 3 shows SAXS intensity distributions in the meridional direction obtained with a PSPC. Curves a and b show profiles from the single-crystal mats SC5 and SC20, respectively, and curve c shows a profile from the undrawn dry gel (UNGEL) film. The distribution of all the specimens shows scattering maxima up to the third order. This indicates that the specimens are composed of lamellar crystals or single crystals highly oriented with their large flat faces parallel to the film surface.

Here it should be noted that the dried gel and single-crystal mats are composed of large lamellar crystals stacked on top of one another to form a periodic structure perpendicular to the plane of the dried gel film. The SAXS intensity distribution from this system has been formulated for two cases; one is based on the concept that the scattering is caused by the excess electron density $\varrho = \varrho_c - \varrho_a$ (ϱ_c and ϱ_a being the electron densities of the crystal and amorphous phases, respectively)[26,27] and the other is that the scattering is caused by positive and negative deviations from the average density of the sample.[28–29] The latter case is thought to be somewhat complicated but realistic. Both treatments provide equations of scattered intensity containing a number of parameters. However, it is difficult to estimate an exact value for all parameters by computer. To avoid such difficulties, fluctuations in the orientation of lamellar crystals and fluctuations of lamellar size were neglected. The analysis was limited to two-phase structures composed of completely oriented lamellar microdomains. Based on these assumptions, attention was focused on quantitatively estimating the boundary (transition) region corresponding to folded loops utilizing SAXS intensity distributions at larger scattering angles than those shown in Figure 3. On subtracting air scattering as well as the scattering arising from the amorphous order and thermal density fluctuations from the total scattered intensity, the residual scattering was assured to be given by a straight line at large scattering angle. Through trial and error, however, it was found that the manner of subtracting the background scattering did not much affect the final value of the density transition at the interface.

The system to be considered here is one which has a one-dimensional electron density fluctuation along a direction normal to the lamellar interfaces and the density variation is periodic. The variation deviates from that of an ideal two-phase system in which the density variation occurs discontinuously from the electron density of the crystal lamellae and voids. If the electron density variation is given by a Gaussian function, the scattered intensity at large angle tail $I(s)$, corrected for background scattering, is given by[30,31]

$$I(s) = \text{const} \times s^{-2} \exp(-4\pi^2\sigma^2 s^2) \tag{1}$$

where

$$s = 2 \sin \theta/\lambda' \tag{2}$$

where λ' is the wavelength of the X-ray beam and 2θ is the scattering angle. σ is a parameter denoting the standard deviation, characterizing the diffuseness of the boundary, and it is related to the interfacial thickness, t, as follows:[30,31]

$$\sigma = (2\pi)^{1/2} t \tag{3}$$

The value of t can be evaluated from the slope and the intercept at $s^{-2} = 0$ in the plot of $\ln(s^2 I)$ vs s^{-2}. The function $I(s)$ corresponds to the scattering intensity from the ideal two-phase system, which is given for isotropic systems as s^{-4} instead of s^{-2} in eq 1 according to Porod's law.[32]

Panels a–c of Figure 4 show the results obtained from SC5, SC20, and UNGEL, respectively. A fairly good linear relationship was obtained experimentally. Table 1 summarizes the periodic distance L evaluated from Figure 3 and the interfacial thickness t calculated from Figure 4. The length L of single-crystal mats SC5 and SC20 is longer than that of UNGEL, while the length t is independent of the given specimens except SC20.

Figure 5 shows the 68 MHz DD ^{13}C NMR spectra obtained by pulse sequence a in Figure 1 for the five types of PE. Here we must emphasize that these spectra were obtained after all the T_{1C} measurements but they are shown first to explain the outline of our NMR experiments. Since the waiting time PD (seconds)

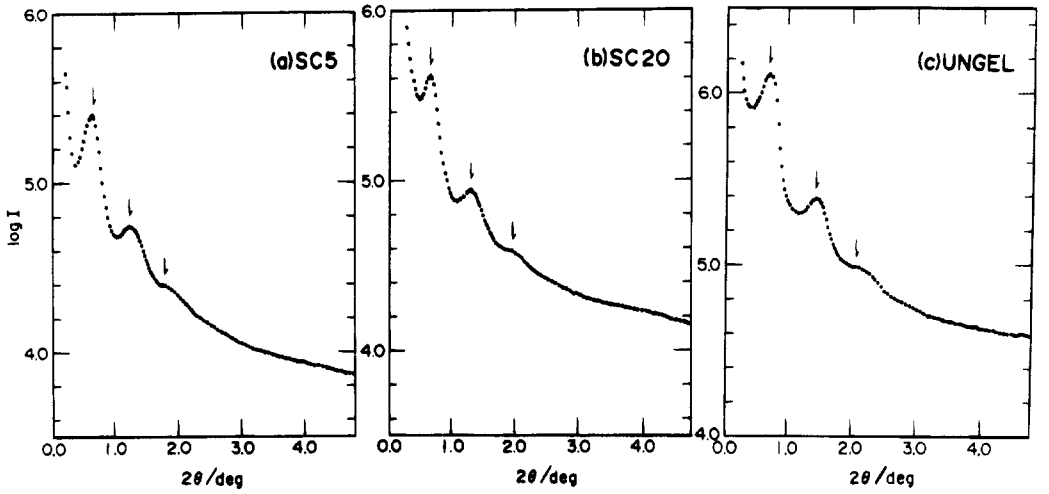

Figure 3. SAXS intensity distribution measured for (a) SC5, (b) SC20, and (c) UNGEL.

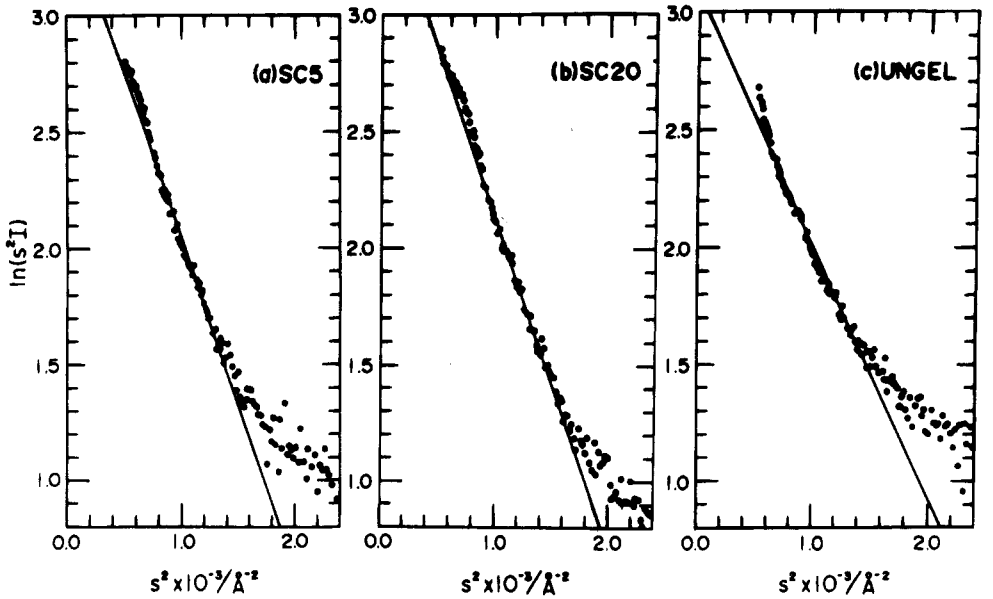

Figure 4. Full analysis of the interfacial thickness, ln $(s^2I(s))$ vs s^2 of (a) SC5, (b) SC20, and (c) UNGEL.

Table 1. Identity Period by X-ray Scattering and Interfacial Thickness Estimated by X-ray Scattering and DD/MAS ^{13}C NMR Spectroscopy

sample	identity period (nm) X-ray	interfacial thickness (nm) X-ray	interfacial thickness (nm) ^{13}C NMR
SC5	14.0	1.51	1.50
SC20	13.6	1.50	0.81
UNGEL ($\lambda = 1$)	12.5	1.51	1.52

was chosen to be longer than 5 times the longest T_{1C} for each sample, these spectra reproduce the contributions from all structural components. In spectum a for the quenched G201 film, two distinct peaks appear at 33 and 31 ppm. As described before, it is well known that the 33 ppm value corresponds to the average of the principal values of the chemical shift tensor for trans–trans methylene sequences of polyethylene and *n*-paraffins in the orthorhombic crystal fom,[13,15,16] while the 31 ppm value is close to the chemical shift observed for n-$C_{17}H_{36}$ in liquid or polyethylene in solution.[17] Thus, we simply assign peaks I and II to the orthorhombic crystalline and noncrystalline components, respectively, according to the concept of Horii et al.[23] In spectra b, c, and d observed for the single-crystal mats, SC5 and SC20, and UNGEL, respectively, the peak at 31 ppm associated with noncrystalline components is indistinct in comparison with the crystalline peak at 33 ppm. This fact is a result of the high degree of crystallinity of these specimens. In addition to the peaks at 33 and 31 ppm, a small peak appeared for ultradrawn polyethylene films; this peak has been reported by Horii et al. to belong to trans–trans methylene sequences in the monoclinic crystal form.[23] Detailed assignment will be discussed later in this paper. As shown in spectrum e for DRGEL ($\lambda = 300$), the peak around 34 ppm was observed clearly as a shoulder of the main peak at 33 ppm.

To inquire whether each resonance line comprises a single component, T_{1C} was measured by the pulse sequence b in Figure 1 developed by Torchia or by the standard saturation–recovery pulse sequence (see pulse sequence c in Figure 1). In doing so, the total magnetizations $M_c(\tau)$ were classified into several components as follows:

For Torchia's pulse sequence

$$M_C(\tau) = 2\sum_{i=1}^{N} M_{cp,i} \exp(-\tau/T_{1C,i}) \qquad (4)$$

For the standard saturation–recovery pulse sequence

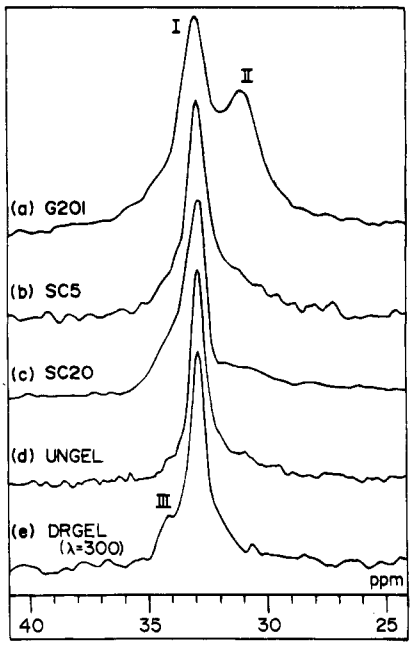

Figure 5. 68 MHz DD/MAS ^{13}C NMR spectra of different polyethylene samples measured by a ($\pi/4$–FID–$3T_{1C}$) single pulse: (a) G201, (b) SC5, (c) SC20, (d) UNGEL, and (e) DRGEL (λ = 300).

$$M_C(\tau) = \sum_{i=1}^{N} M_{cp,i}(\infty)\{1 - \exp(-\tau/T_{1C,i})\} \qquad (5)$$

where $M_{cp,i}$ is the ^{13}C magnetization of the ith component after CP and $M_{C,i}(\infty)$ is the equilibrium ^{13}C magnetization of the ith component. To satisfy eq 4, ^1H magnetization must be zero or constant. For this purpose, the proton magnetization during τ must be saturated by a string of $^1H90°$ pulses with a constant interval of t with a suitable value which satisfies the relationship $T_{2H} < t < T_{1H}$. The suitable value was set in the range 10–20 ms for each specimen. For T_{1C} beyond several thousand seconds, however, $^1H90°$ multiple pulses beyond several houndred thousand times must be applied during τ with a time scale > $2T_{1C}$. To avoid this technical difficulty in measuring T_{1C} and to ensure the recovery of ^1H magnetization, the interval of t was set to several hundred milliseconds and the value of PD was chosen to be longer than 5 times the longest T_{1H} for each specimen.

Figures 6 and 7 show examples for the semilogarithmic plot of the ^{13}C magnetization of the peak height of the line at 33 ppm pictured in Figure 5 as a function of τ for SC20 and DRGEL, respectively. The overall decay curve a in Figure 6 measured for single-crystal mat SC20 can be classified into three components by using a least squares method with a computer: a slow decay curve a, an intermediate decay curve b, and a rapid decay curve c. The initial slope of each decay curve yields T_{1C}. Figure 7 shows the results for DRGEL. The overall decay curve can also be classified into three components.[23] The results obtained from Figures 6 and 7 for the orthorhombic crystal form are listed together with the T_{1C} values of the other specimens in Table 2.

As for peak III relating to the monoclinic crystal form, the measurements could be convenient only for DRGEL by Torchia's pulse sequence.[25] Actually, the X-ray diffraction from the monoclinic crystal has been confirmed at 19.6° (twice the Bragg angle), lower than the diffraction angle (21.6°) of the (110) plane of the orthorhombic crystal form.[32] A linear relationship of the semiloga-

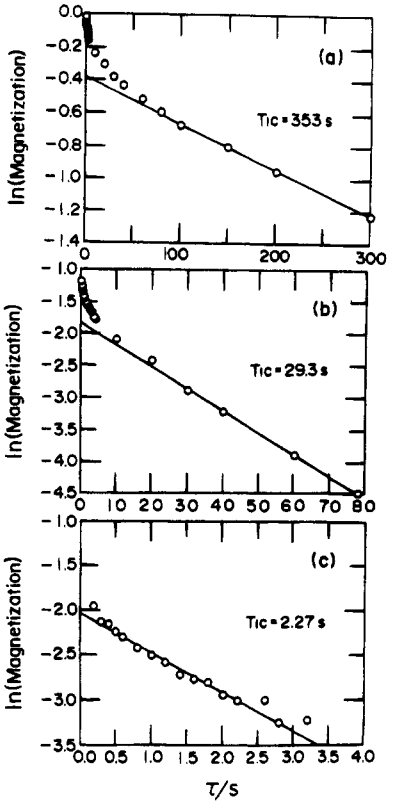

Figure 6. Semilogarithmic plot of the ^{13}C magnetization of the peak height of the line at 33 ppm for SC20 pictured in Figure 5.

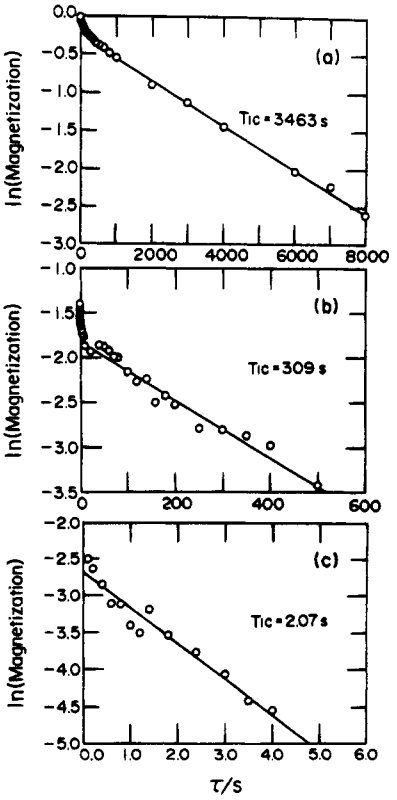

Figure 7. Semilogarithmic plot of the ^{13}C magnetization of the peak height of the line at 33 ppm for DRGEL pictured in Figure 5.

rithmic plot of magnetization by Torchia's pulse sequence could be maintained, indicating a single pulse of T_{1C} when the waiting time PD was set to a value larger than 5 times T_{1C}.

For T_{1C} measurements relating to the noncrystalline phase, peak II in Figure 5 was performed in the range

Table 2. ^{13}C Spin–Lattice Relaxation Time (T_{1C}) and Spin–Spin Relaxation Time (T_{2C}) for Different Kinds of Polyethylene Specimens

	T_{1C} (s)					T_{2C} (μs)	
	crystalline component					noncrystalline component	
specimen	orthorhombic			monoclinic	noncrystalline component	interfacial	rubbery
G201	145	15.8	1.27		0.375	40	2535
SC5	900	228	4.04		0.452	45	1207
SC20	353	29.3	2.27		0.412	38	2286
UNGEL	1017	187	2.50		0.570	40	486
DRGEL	3463	310	2.10	1726			

$0.05 < \tau < 5$ s by the standard saturation–recovery pulse sequence (see pulse sequence c in Figure 1). For the four specimens except the quenched G201 film, the magnitude of peak II appearing in the DD ^{13}C spectrum is lower than that of peak I, indicating a high crystallinity of the test specimen. Peak II is strongly affected by peak I for $\tau > 1.0$ s, and then the logarithm of ^{13}C magnetization vs τ deviates from a linear relationship. At $\tau < 0.5$ s, a linear relationship was obtained for SC5, SC20, and UNGEL, and T_{1C} has been estimated by the usual decay analysis—the semilogarithmic plot of the ^{13}C magnetization against τ. On the other hand, in spite of our varying values of τ in the sequence of Figure 1c, no 31 ppm peak intensity could be observed for DRGEL, indicating extremely high crystallinity. These results are also summarized in Table 2. It is seen that the crystalline components at 33 ppm show significant ranges of variability for each of the T_{1C}: 140–3500, 15–310, and 1–4.1. It is incorrect to assign the shortest T_{1C} value as the noncrystalline component. The noncrystalline component for all the specimens except UNGEL obtained by pulse sequence c in Figure 1 had a single value of T_{1C} as short as 0.3–0.6, indicating that the noncrystalline region is homogeneous in the relatively high-frequency molecular motions which determine the T_{1C} value. Incidentally, the shortest T_{1C} values measured by Torchia's pulse sequence[25] were in fairly good agreement with those measured by the standard saturation–recovery pulse sequence for peak I. The value of T_{1C} for the monoclinic crystal form in the DRGEL is about one-half of the corresponding T_{1C} of the orthorhombic crystals. This indicates greater molecular mobility in the slightly larger unit cell of the monoclinic crystals.

Figure 8 stacked spectra of the quenched G201 films for different values up to 400 μs obtained by pulse sequence d in Figure 1 with PD = 3 s. Here, the contribution from crystalline components with T_{1C} values of 145 and 15.8 s is strongly suppressed because of the short values of τ. The spectrum taken with $\tau <$ 80 μs is postulated to contain all noncrystalline components and a part of the crystalline component with T_{1C} = 1.27 s. When τ increases beyond 56 μs, the spectra show a single peak. This indicates that the contribution from the crystalline and noncrystaline components with shorter transverse relaxation times rapidly disappears, leaving only the contribution from the noncrystalline component with a longer transverse relaxation. Thus only a single peak remains at 31 ppm, and the line shape remained essentially unchanged except for a slight broadening. Accordingly, the line with the peak position at 31 ppm can be assigned to the rubber-like amorphous component with active molecular mobility.

Figure 9 shows the semilogarithmic plot of the peak heights of the line at 31 ppm as a function of τ shown in Figure 8. The overall decay curve a can be clearly

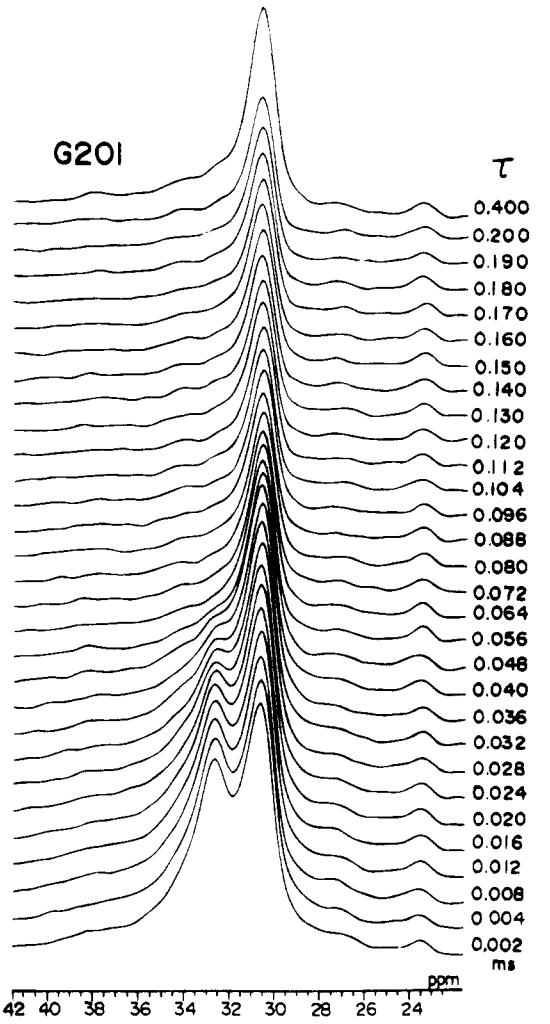

Figure 8. Stacked spectra of the quenched G201 obtained by pulse sequence d.

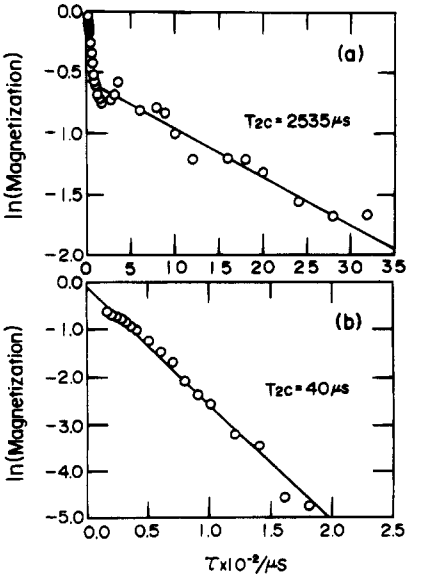

Figure 9. Semilogarithmic plot of the ^{13}C magnetization of the peak height of the line at 31 ppm for the quenched G201 as a function of τ in Figure 8.

resolved into two parts, a rapid decay within 200 μs and a subsequent slow decay. The initial slope of the slower decay yields T_{2C} = 2535 μs, while T_{2C} of the rapid decay was estimated to be 40 μs by the usual decay analysis. These two decays do not contain any contribution from the crystalline component, because the overlap of the

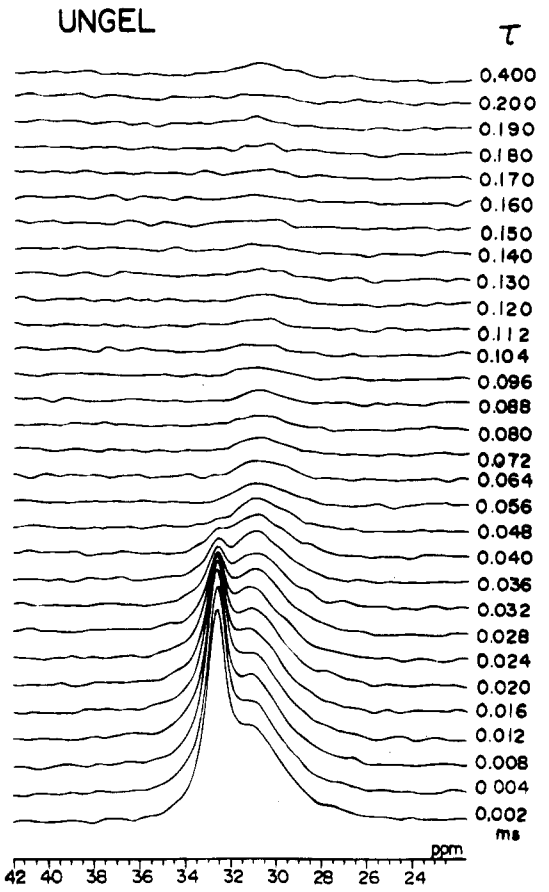

Figure 10. Stacked spectra of the quenched UNGEL obtained by pulse sequence d.

crystalline 33 ppm line on the line at 31 ppm is negligibly small even in the spectra taken with the indicated τ values. The component with $T_{2C} = 2535$ μs is recognized as the rubber-like amorphous component, while that with $T_{2C} = 40$ μs is much less mobile than the amorphous component. Therefore, this component can be assigned to the interfacial noncrystalline component in consideration of the lamellar structure.

Figure 10 shows stacked spectra for UNGEL films. The τ-dependence of the spectra is different from that of the quenched G201 films shown in Figure 8. Even for the spectrum taken with $\tau = 2$ μs, the contribution of a part of the crystalline component with $T_{1C} = 2.5$ s is more significant than that of all noncrystalline components, indicating a higher crystallinity for this test specimen than for the G201 films. At $50 < \tau < 88$ μs, only a small, somewhat broadened peak at 31 ppm associated with the noncrystalline component remains. The single line cannot be resolved from the rolling baseline, indicating that the decay of the amorphous component for the UNGEL film is much faster than that of the quenched G201 films. With further increase in τ beyond 92 μs, all the contributions from the crystalline and noncrystalline components with shorter transverse relaxation times disappeared. In spite of the complicated stacked spectra, the semilogarithmic plots of the peak height at 31 ppm could be measured and two kinds of decays could be obtained using the same method as described in Figure 9. The two contributions related to the amorphous and interfacial noncrystalline phases are summarized in Table 2 for all the specimens except DRGEL. As for DRGEL, measurements of T_{2C} were impossible because of extremely high crystallinity; measurements on DRGEL shall be described briefly later.

According to Table 2, it is seen that the orthorhombic regions are made up of three components with different T_{1C} values for all the specimens. On the other hand, the noncrystalline region consists of two phases with different molecular mobilities for all specimens except DRGEL. For DRGEL, the T_{1C} value of the monoclinic crystal form was observed, while the T_{2C} value of the noncrystalline region could not be observed.

Now, we shall refer to the problem for estimating T_{1C} in the present paper. Schmidt-Rohr and Spiess have reported that solid-state chain diffusion between the crystalline and noncrystalline regions in linear polyethylene at temperatures down to −173 °C is detected by means of two-dimensional and one-dimensional exchange ^{13}C NMR experiments under the MAS condition.[33] They explained chain diffusion in terms of the nuclear Overhauser enhancement factor (NOEF) and the nonexponential T_{1C} in the crystallites, as well as the dependence of T_{1C} on the crystallite thickness reported by Axelson et al.,[34] by excluding the possibility of ^{13}C spin diffusion to the exchange of magnetization between the amorphous and crystalline regions. If this is the case, our results contain an ambiguous point: a question arises as to whether the orthorhombic crystal form consists of three components. Except at temperatures lower than the glass transition temperature, one can consider one possibility that the ^{13}C magnetization for the orthorhombic crystal form is really a continuum of T_{1C} values; the short T_{1C} component arises from those initially crystal carbons which migrate quickly into the noncrystalline regions and relax, while the long T_{1C} component presumably arises from carbons initially found in the interior of the crystal. If the chain diffusion occurs mainly at the exterior of the orthorhombic crystals and consequently the orthorhombic crystals exhibit different morphology at the exterior and interior (which has neven been detected by X-ray diffraction), the ^{13}C magnetization represented as a continuous curve is thought to be apparently classified into three components: a slow decay curve, an intermediate decay curve, and a rapid decay curve.

Based on a series of experimental results, the total spectra in Figure 5 were analyzed in terms of the contribution of these components to determine the mass fractions. To this end, we have first determined the line shape of the interfacial component centered at 31.1−31.8 ppm by the subtraction of spectra. The procedure for the quenched G201 films is shown in Figure 11. Here, spectrum A obtained at PD = 3 s in pulse sequence a in Figure 1 represents the contribution from all the noncrystalline components and a minor contribution from the crystalline component with $T_{1C} = 1.27$ s corresponding to the fastest decay (see Table 2). Spectrum B is a reproduction of the spectrum at $\tau = 0.4$ ms of Figure 8. As discussed before, this spectrum with the peak at 31 ppm reveals the contribution from the rubber-like amorphous component. When spectrum B is subtracted from spectrum A, spectrum C is obtained. This spectrum is attributed to the interfacial noncrystalline component as well as the crystalline component with the fastest decay. A crude knowledge of peak positions is important for expediting the component analysis algorithm by computer. Line shape analysis of spectrum C was done by using a complex function given as a combination of Gaussian and Lorentzian functions. The highest peak of spectrum C was at 31.5 ppm.

After determining the peak position of spectrum C, spectrum A was classified into three complex functions by least-squares fitting; the line width and the peak

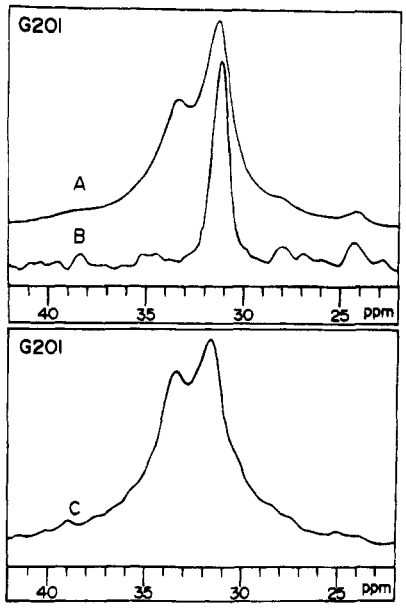

Figure 11. Analysis of the DD/MAS ^{13}C NMR spectrum of the quenched G201: (A) the noncrystalline spectrum measured by PD = 3 s; (B) the spectrum of the rubbery component at τ = 300 μs in Figure 8; (C) the spectrum obtained by the subtraction of spectrum B from spectrum A.

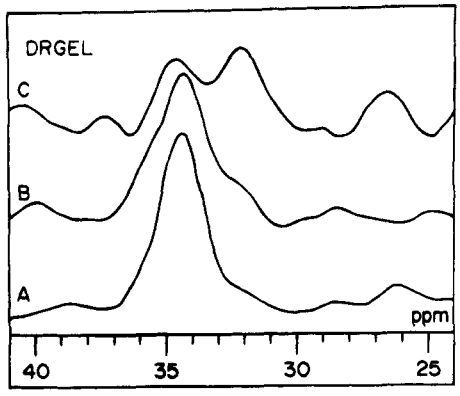

Figure 12. Analysis of the DD/MAS ^{13}C NMR spectrum of the DRGEL (λ = 300): (A) the spectrum at τ = 3 μs among the stacked spectra; (B) the spectrum at τ = 17 μs among the stacked spectra; (C) the spectrum at τ = 41 μs among the stacked spectra.

height of each component were varied while keeping the peak positions of 33.0, 31.5, and 31 ppm for the crystalline, interfacial, and rubbery components. The curve summarized by the three complex functions was in good agreement with the observed spectrum A. The same analysis was done for SC5, SC20, and UNGEL, and good agreements were also obtained. This symmetrical lineshape analysis for the three components plays an important role in pursuing curve fitting of the DD ^{13}C spectrum (see Figures 13 and 14).

Incidentally, the peak position of the monoclinic line could only be obtained for DRGEL; this position was used as an initial value for other specimens whose peak position could not be detected in stacked spectra.

Figure 12 shows stacked spectra A, B, and C taken with τ = 3, 17, and 41 μs, respectively, for DRGEL (λ = 300)[23] by using pulse sequence d in Figure 1. These spectra were obtained by the accumulation of 500 times. Unfortunately, the spectra showed considerable baseline noise, which obviously indicates the difficulty in measuring the T_{2C} value for DRGEL films with very small noncrystalline components (see Table 2). As can be seen in Figure 12, spectrum A shows a single peak around

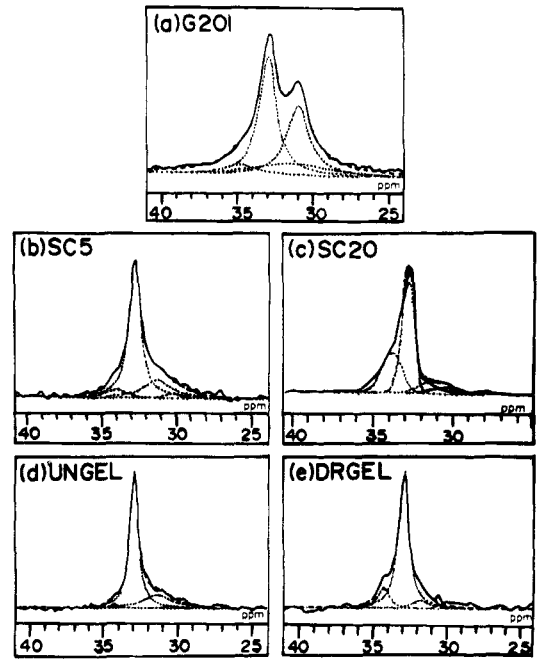

Figure 13. Component analysis of the total spectra for different polyethylene samples shown in Figure 5: (a) G201; (b) SC5; (c) SC20; (d) UNGEL; (e) DRGEL (λ = 300).

34.2 ppm. Judging from the chemical shifts,[23] this peak obviously arises from the monoclinical crystal form, which has been confirmed by X-ray diffraction. This indicates that the noncrystalline component was concealed because of strong residual magnetization of the monoclinic crystal form. With increasing τ up to 17 μs, the contribution from the noncrystalline component could be observed as a shoulder around 31.8 ppm. This peak becomes clearer as τ increases. At τ > 41 μs, however, the peak quickly became indistinct and then disappeared, indicating that the contribution from the rubbery state can be ruled out. Thus, it turned out that this peak is attributed to the contribution of the interfacial noncrystalline component. The spectrum at τ = 41 μs was found to be the best one to observe the interfacial component.

The DD ^{13}C spectrum in Figure 5 was analyzed by least-squares fitting in terms of three parameters of the complex function given as Gaussian and Lorentzian functions, in which the line width and the peak height of each component were determined on the basis of small changes from the initial peak position, which was done to give the best fit by computer. The initial values of the orthorhombic crystal, interfacial, and rubbery components were determined using the method described in Figure 11, and the initial value of the monoclinic crystal form was set to 34.2 ppm measured for DRGEL in Figure 12. Although the line corresponding to the orthorhombic crystal form at about 33 ppm consists of three components with different T_{1C}, each component was assumed to have a single line shape. The purpose of the analysis of the spectrum is to estimate crystallinity by ^{13}C NMR on the basis of the experimental results that the integrated fraction of the crystalline line is in good accord with the degree of crystallinity estimated by ^{1}H broad-line NMR analysis and the latter coincides with values obtained from density measurements.[35,36] The results are shown in Figure 13, where the integrated fractions of the respective components are also shown as a dashed line. The composite curve is shown by a dotted line, which reproduces well the observed spectrum (a solid line). The

Table 3. ^{13}C Chemical Shifts and Mass Fractions of the Respective Components for Different Kinds of Polyethylene Specimens

	chemical shift (ppm)				mass fraction (%)			
specimen	C_O[a]	C_m[b]	I[c]	R[d]	C_O[a]	C_m[b]	I[c]	R[d]
G201	33.0	34.9	31.5	31.0	43.8	6.92	16.1	33.2
SC5	32.9	34.3	31.4	30.4	67.1	8.02	21.5	3.43
SC20	32.8	33.7	31.5	30.5	49.4	28.9	12.2	9.50
UNGEL	32.9	34.2	31.4	30.6	72.8	1.55	24.3	1.34
DRGEL	32.9	34.3	31.8	30.5	78.8	12.7	6.94	1.58

[a] C_O, orthorhombic crystal form. [b] C_m, monoclinic crystal form. [c] I, interfacial component. [d] R, rubbery component.

Table 4. Crystallinity Measured by ^{13}C NMR and Density with Different Kinds of Polyethylene Specimens

	crystallinity (%)	
specimen	^{13}C NMR	density
G201	58.7	38.1
SC5	85.8	87.0
SC20	85.7	82.0
UNGEL	86.5	86.0
DRGEL	95.0	96.0

integrated intensity fraction and the corresponding chemical shifts thus obtained are listed in Table 3.

It is seen that the chemical shift of each component is almost independent of the specimen type except for a slight difference for the monoclinic crystal form in SC20. The mass fraction of the latter was less than 13% for DRGEL (λ = 300) in spite of the observable X-ray diffraction intensity from monoclinic crystals.[37] In contrast, the mass fraction of the monoclinic crystal form was 28.9% for SC20, although the monoclinic crystal form has never been observed by X-ray diffraction.[24] This contradiction is thought to be due to the fact that the component at 33.8 ppm for SC20 is associated with unstable parts of orthorhombic crystals rather than well-formed monoclinic crystals. On the other hand, the rubber-like amorphous component is negligibly small in DRGEL. This is in good agreement with results of density and X-ray diffraction measurements. The thickness t of the interfacial noncrystalline region was calculated by $Lw/2$, where L is the long period and w is the mass fraction of the interfacial noncrystalline component.[21] The results are listed in Table 1 together with the X-ray diffraction results. Interestingly, the interfacial thickness estimated by ^{13}C NMR is almost equal to that estimated by X-ray diffraction except for SC20. This indicates that the estimation of the phase structure by ^{13}C NMR is reasonable.

Here it may be noted that the total mass fraction of the orthorhombic and monoclinic crystal forms can be estimated as the crystallinity of the given specimen. The results are listed in Table 4. It is seen that except for G201 the crystallinity estimated by ^{13}C NMR is in good agreement with that by density. This indicates that ^{13}C NMR has an advantage in determining the phase structure of a crystalline polymer. Furthermore, the exact estimation for the mass fraction in the interfacial region by X-ray scattering (see Table 1) is generally difficult except when crystal lamellae are highly oriented with large flat faces and the difference of densities between the crystal and amorphous regions is very large. Accordingly, the estimation of the interfacial thickness was impossible by X-ray diffraction for specimens like the quenched G201 and DRGEL (λ = 300). However, ^{13}C NMR gives the mass fraction of the interfacial noncrystalline component. Furthermore, the crystallinity by density measurement must be estimated on the basis of the simple assumption that the specimen consists of two phases, the crystalline and the noncrystalline phases. Thus the density measurements cannot provide any information about the interfacial region.

Here we must point out an ambiguity in determining the T_{2C} of the interfacial noncrystalline component. Returning to Figure 9, it is seen that T_{2C} could be estimated from the rapid decay of the overall decay curve which was obtained by the semilogarithmic plot of the peak height of the line at 31 ppm corresponding to the rubber-like amorphous component. The peak for the interfacial noncrystalline component was determined at about 31.5 ppm by the analysis of the DD ^{13}C spectrum shown in Figure 13, but no peak at 31.5 ppm could be observed directly for measuring T_{2C}. For this reason, we judged that the overall decay curve measured at 31 ppm contains the contribution of the interfacial noncrystalline component, since the overall decay curve could be clearly classified into the rapid decay and slow decay indicating quite different mobile characteristics.

Another advantage of ^{13}C NMR is the determination of crystallinity at elevated temperatures, since the estimation of crystallinity at various temperatures by density measurements is impossible. The temperature dependence of crystallinity is of interest for understanding why the Young's modulus of crystalline polymers decreases with temperature, although such a finding is common in polymer science. In accordance with our previous work using ultradrawn polyethylene and polypropylene films,[10] we found the crystal lattice moduli of polyethylene and polypropylene in the chain direction to be independent of temperature up to the melting point within experimental error in spite of the drastic decrease in the Young's modulus. Judging from the decrease in X-ray diffraction intensity with temperature, the decrease in the Young's modulus was thought to be due to the decrease in crystallinity with temperature. However, quite different results have been reported for the temperature dependence of crystallinity. For example, Spiess et al. suggested that crystallinity remains constant over a wide temperature range on the basis of molecular motion studied by ^2H wide NMR spectroscopy.[38] In contrast, McBrierty and McDonald postulated a 10% reduction in crystallinity at 60 °C as a way to give the best fit between experimental and theoretical values by assuming simple additivity of each contribution of the crystal and amorphous phase to the total second-order moment of the resonance absorption.[39]

Based on the above different concepts, it may be expected that the fully relaxed DD ^{13}C spectrum would offer a good means for estimating the temperature dependence of crystallinity. Furthermore, it is of interest to study whether the values of T_{1C} and T_{2C} for the crystalline and noncrystalline components by ^{13}C NMR measurements are sensitive to the temperature dependence of the crystal lattice modulus and Young's modulus. Before the measurements, all the specimens were annealed to improve their crystallinity as much as possible in order to avoid their thermal crystallization. Incidentally, ^{13}C NMR measurements were carried out in the same manner as already described for room temperature.

In doing so, however, it is important to check whether spectra of T_{1C} and T_{2C} at temperatures >70 °C associated with the α mechanism[40] ensure a symmetrical line shape and the line for the orthorhombic crystal form which consists of three components with different T_{1C} can be assumed to have a single peak. For example, if crystalline carbons closer to the interfacial noncrystal-

Table 5. ^{13}C Spin–Lattice Relaxation Time (T_{1C}) and Spin–Spin Relaxation Time (T_{2C}) as a Function of Temperature for Three Kinds of Annealed Polyethylene Specimens

		T_{1C} (s)					T_{2C} (μs)	
		crystalline component				noncrystalline component	noncrystalline component	
specimen	temp (°C)	orthorhombic			monoclinic		interfacial	rubbery
G201	27–40	267	29.0	1.39		0.464	40	2500
	54–60	200	26.0	2.22		0.507	59	4545
	88–93	117	19.0	1.33		0.672	83	10000
UNGEL	27–40	1213	200	3.30		0.576	34	416
	54–60	491	117	3.22		0.995	34	756
	88–93	241	28.0	3.44		1.36	36	866
DRGEL	27–40	3463	310	2.10	1726	0.444		
	54–60	3104	304	2.48		0.612		514
	88–93	2398	285	2.46		0.734		619

line region undergo a transition from a trans conformational state to a gauche one by the chain diffusion, it may be expected that the peak shifts toward high field which develops for the crystalline line shape. For the orthorhombic crystal form, the overall decay curve at temperatures <70 °C could be easily classified into three components from the semilogarithmic plot of the ^{13}C magnetization of the peak height of the line at 33 ppm as a function of τ as shown in Figures 6 and 7 as the results at room temperature. For the G201 specimen at 88–93 °C, we could recognize a small peak at about 33 ppm, similar to the shoulder of the large peak of the noncrystalline components but could not confirm the peak shift. Such an indistinct peak indicates the difficulty in measuring the T_{1C} value. Accordingly, the measurements at the indicated temperature range were carried out several times to check the reproducibility of the T_{1C} values and the values were determined using an overall decay curve ensuring a smooth profile. To obtain the peak position of the noncrystalline component, stacked spectra similar to those in Figure 8 or 10 could be observed at elevated temperatures for G201 and UNGEL. With increasing τ, the spectra showed a single peak at around 31 ppm, indicating only a contribution from the rubber-like amorphous component. Analysis of the peak height at 31 ppm versus τ gave plots like those of Figure 9, which suggested two decay constants, a rapid decay, 34–83 μs and a slow decay, 400–10000 μs. By using the method described for the explanation of Figure 11, the peak position of the interfacial noncrystalline component was also determined, which was about 31.5 ppm, but the peak shift with temperature could not be recognized because of the baseline noise of the spectrum. Nevertheless, the spectrum obtained at PD = 3 s in pulse sequence a in Figure 1 measured for G201 and UNGEL at elevated temperatures was classified into three complex functions by keeping the peak positions of 33.0, 31.5, and 31 ppm for the crystalline, interfacial, and rubbery components as already described for the measuements at room temperature. At 88–93 °C, the agreement between the curve summarized by the three complex functions and the observed spectrum becomes slightly worse than that measured at lower temperatures, indicating the derivation from the symmetrical line shape of each spectrum. Interestingly, for DRGEL at 88–93 °C, an indistinct small peak at 31 ppm was observed in the stacked spectra with increasing τ, indicating an increase in the noncrystalline components. Even so, the indistinct small peak was too small to do the treatment shown in Figure 11 and the peak position of the interfacial noncrystalline component was determined to be about 31.5 ppm by using the same treatment as in Figure 12. Of course, any treatment was impossible at temperatures >95 °C.

Table 5 shows the temperature dependence of T_{1C}. The observed temperatures cover ranges because of the fluctuation during the measurements. It is seen that the orthorhombic crystal form has three different values of T_{1C} for all the specimens in the given temperature range. Comparing Table 5 with Table 2 at 27–40 °C, the T_{1C} values for the annealed G201 films and UNGEL films are larger than those for the quenched films at room temperature. This suggests that the number of defects within crystallites decreases and the average crystal size becomes larger through the annealing. For DRGEL gel films (λ = 300), the values at room temperature listed in Table 2 are listed again in Table 5.

With increasing temperature, the longest T_{1C} value among the three components associated with the typical crystalline phase became shorter, reflecting more active chain mobility. In contrast, the value of T_{1C} for the noncrystalline component becomes longer with temperature.

The temperature dependence of the molecular mobility could be confirmed by examining T_{2C} behavior. The resulting T_{2C} values are listed in Table 5. The value for the annealed G201 films tends to increase with temperature, indicating active mobility of molecular chains. This tendency is obviously considerable for the rubber-like amorphous component, indicating an active molecular mobility like that of a high-viscosity fluid rather than a soft solid. For the annealed UNGEL films, the T_{2C} value of the rubber-like region increased with temperature, while that of interfacial region is almost independent of temperature. This means that the rubbery state of UNGEL films with a morphology similar to that of single-crystal mats exhibits characteristics like those of a very soft solid or a very high viscosity fluid at elevated temperature, while the constraints on mobility are much higher and independent of temperature in the interfacial region. According to the SAXS patterns, the long period of about 12 nm observed for original (not annealed) films becomes greater than 30 nm through annealing at temperatures above 120 °C,[32] in spite of the small increase in crystallinity. Even so, the large change in lamellar thickness at elevated temperature did not give rise to the molecular mobility of the interfacial region within the annealed dry gel films. For the DRGEL films, the contribution from the noncrystalline region could not be detected in the stacked spectra at room temperature as listed in Table 2, but with increasing temperature the increase in the T_{2C} value was detected. This is attributed to an increase in mass fraction of the noncrystalline region. In any case, the molecular mobility of the noncrystalline region within the three different annealed PE specimens becomes more pronounced with temperature.

Figure 14 shows the DD ^{13}C spectra for the three annealed specimens, G201, UNGEL, and DRGEL films (λ = 300), at various temperatures. The line shape

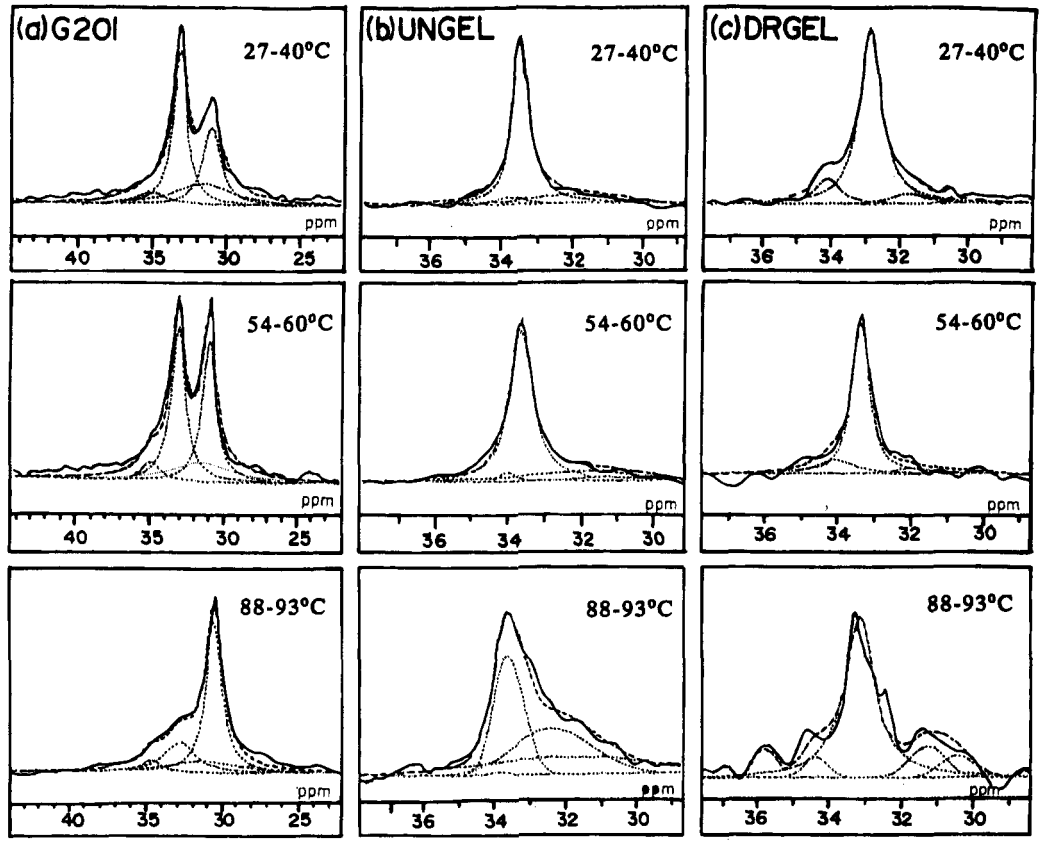

Figure 14. Component analysis of the total spectra for different annealed polyethylene samples: (a) G201; (b) UNGEL; (c) DRGEL ($\lambda = 300$).

Table 6. ^{13}C Chemical Shifts and Mass Fractions of the Respective Components as a Function of Temperature for Different Kinds of Annealed Polyethylene Specimens

specimen	temp (°C)	chemical shift (ppm)				mass fraction (%)			
		C_O[a]	C_m[b]	I[c]	R[d]	C_O[a]	C_m[b]	I[c]	R[d]
G201	27–40	33.0	34.8	31.5	30.9	41.2	7.2	23.7	27.9
	54–60	33.1	34.9	31.5	30.9	38.8	6.6	19.4	35.2
	88–93	33.0	34.8	31.4	30.7	21.5	5.5	17.4	55.6
UNGEL	27–40	33.5	33.8	31.8	30.6	74.3	4.0	21.1	0.6
	54–60	33.5	34.0	31.8	30.8	72.1	2.2	19.8	5.9
	88–93	33.5	33.8	32.3	31.9	35.0	0.9	35.5	28.6
DRGEL	27–40	33.0	34.0	30.9	30.1	78.8	12.7	6.9	1.5
	54–60	33.4	34.0	31.9	30.1	74.9	14.3	7.7	3.2
	88–93	33.2	34.4	31.4	30.6	74.0	5.3	12.6	8.2

[a] C_O, orthorhombic crystal form. [b] C_m, monoclinic crystal form. [c] I, interfacial component. [d] R, rubbery component.

deconvolution was done by using the same method as described in Figure 13. Each composite curve is shown by a dotted line, which reproduces well the observed spectrum except for the DRGEL film at 88–93 °C. However, this analysis was done to compare the temperature dependence of crystallinity with those estimated by X-ray diffraction. The integrated intensity fraction and the chemical shifts are listed in Table 6. It is seen that the chemical shift of each component is almost independent of change in temperature for all the specimens within experimental error. The mass fraction is sensitive to an increase in temperature. For the crystalline region, the mass fraction of the monoclinic crystal form decreases with temperature, indicating a phase transition to either the orthorhombic crystal or the noncrystalline component. Since the orthorhombic crystal form is thermodynamically more stable than the monoclinical crystal form, the additional mobility at higher temperatures allows chains to find their true energy minima. The mass fraction of the orthorhombic crystal form decreases with temperature but the degree

Table 7. Crystallinity Measured by ^{13}C NMR and Density as a Function of Temperature for Different Kinds of Annealed Polyethylene Specimens

specimen	temp (°C)	crystallinity (%)		
		^{13}C NMR	density	X-ray
G201	20		38.1	55.3
	27–40	48.4		
	40			54.1
	54–60	45.4		
	70			50.7
	88–93	27.0		
	90			48.4
UNGEL	20		89.0	
	27–40	78.3		
	54–60	74.3		
	88–93	35.9		
DRGEL	20		96.2	96.2
	27–40	91.5		
	50			96.0
	54–60	89.2		
	70			94.0
	88–93	79.3		
	100			87.0

is sensitive to the morphology of the test specimens. That is, the crystallinities for the two kinds of specimens, G201 and UNGEL films, decrease drastically with increasing temperature up to 90 °C. In contrast, the crystallinity of the DRGEL film exhibits a gradual decrease with temperature. This suggests that the heat resistance of the extended crystal is more significant than that of the folded type crystal.

Table 7 summarizes the temperature dependence of crystallinity estimated from the DD ^{13}C spectra. The results from the DD ^{13}C spectra indicate that crystallinity decreases with increasing temperature. To check this phenomenon, the crystallinity for the three specimens was also estimated by X-ray diffraction using Ruland's method.[41–43]

Figure 15 shows appearance of X-ray diffraction intensity as a function of s ($s = 2\pi \sin\theta_B/\lambda'$, where θ_B is the Bragg angle and λ' is the wavelength) for the annealed G201 specimen at the indicated temperatures. The curves were obtained by subtracting the air scattering, polarization absorption, and incoherent scattering from the observed intensity. To obtain the diffraction intensity from the crystal phase after the above corrections, the intensity curve was separated into the amorphous contribution and the contribution from the individual crystal planes obtained on the basis of the assumption that eack peak from crystal planes had a symmetric form given by a Lorentzian function. The solid line represents the total contribution from the crystalline and noncrystalline phases, and the dotted line represents the contribution from the noncrystalline phase after subtracting the summation of intensity curves of each crystal plane.

According to Ruland[41-43] and Killian,[44] the crystallinity for an undrawn film can be obtained as follows:

$$X_{cr} = X'_{cr}K \tag{6}$$

where, X'_{cr} and K are given by

$$X'_{cr} = \int_{S_0}^{S_p} s^2 I_{cr}(s)\, ds / \int_{S_0}^{S_p} s^2 I(s) ds \tag{7}$$

and

$$K = \int_{S_0}^{S_p} s^2 \langle f^2 \rangle\, ds / \int_{S_0}^{S_p} s^2 \langle f^2 \rangle D_t^2\, ds \tag{8}$$

where

$$\langle f^2 \rangle = \Sigma n_j f_j^2 / \Sigma n_j \tag{9}$$

$I_{cr}(s)$ and $I(s)$ in eq 7 are the intensity distributions from the crystal and the specimen, respectively. s_0 is the value associated with the initial scanning angle, and s_p is related to the desired scanning angle for determining the crystallinity. f_j is the scanning factor of the jth atom, and n_j is the number of atoms within a crystal unit. Therefore, $\langle f^2 \rangle$ means the average scattered intensity from the atoms. D_t is the coefficient containing the first- and second-order lattice distortion associated with thermal fluctuation, which is given by

$$D_t^2 = \exp\{-ks^2\} \tag{10}$$

Table 8 shows the temperature dependence of crystallinity of G201 films obtained by using Ruland's method, which has been previously applied to polypropylene.[42] The value of k must be determined to give a constant value of crystallinity which is independent of the integrated region ($s_0 - s_p$). Such a value was chosen by computer, instead of the preparation of a monogram proposed by Ruland.[43] The crystallinity decrease with increasing temperature but the value at room temperature is higher than that measured by density shown in Table 3.

The results at elevated temperature are summarized in Table 7 together with results obtained by other methods. Incidentally, the changes in crystallinity for DRGEL films ($\lambda = 300$) measured for the (002) plane described elsewhere[21] are listed together in this table. The results by X-ray diffraction are in good agreement with those estimated by ^{13}C NMR. The small difference is probably due to the different experimental conditions: the ^{13}C NMR data were obtained with the length allowed to change freely during the measurement at elevated temperature, while the X-ray data were obtained with fixed length by clamping the film between two metallic clamps. In our NMR instrument, it was impossible to set the specimen with fixed length in the cylinder type sample tube. In any case, it is evident that the crystallinity of the annealed PE films decreases with temperature. This phenomenon suggests one of the most important conclusions that the decrease in Young's modulus is related to the decrease in crystallinity and the decrease in the elastic modulus of the noncrystalline region, since the crystal lattice modulus detected by the X-ray diffraction technique is independent of temperature within experimental error. This mechanism has been already demonstrated by the crude estimation of the temperature dependence of crystallinity by X-ray diffraction[20] but this concept was also confirmed through the ^{13}C NMR in detail. Incidentally,

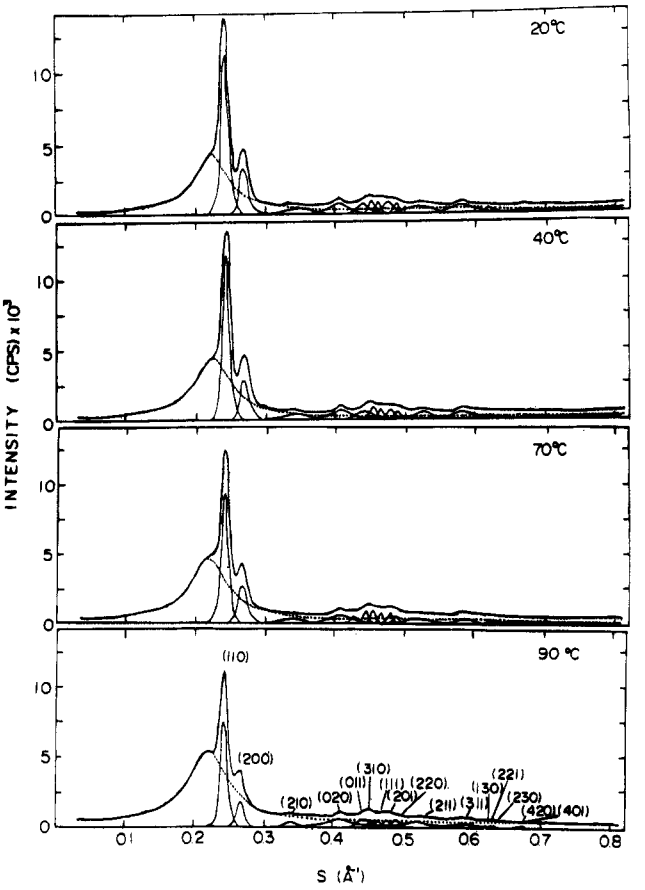

Figure 15. X-ray diffraction diagrams of the annealed G201 specimen measured at the indicated temperatures: thick solid curve, total contribution from crystal and noncrystalline phases; thin solid curve, contribution from each peak from the crystal planes; dotted curve, contribution from noncrystalline phase.

Table 8. Crystallinity for the Annealed G201 Specimen Calculated by $k = 0$ and a Desired Value of k To Give a Constant Value in the Integrated Region of ($s_0 - s_p$) using the Ruland Method

integrated region ($s_0 - s_p$)	temperature (°C)						
	20		40	70		90	
	$k = 0$	$k = 0.6$	$k = 0$	$k = 0$	$k = 0.4$	$k = 0$	$k = 0.38$
0.03–0.596	51.6	54.3	52.6	48.8	50.5	33.3	47.6
0.03–0.636	52.7	55.9	54.3	49.7	51.7	33.2	49.6
0.03–0.676	52.5	56.0	54.7	49.4	51.5	31.8	49.6
0.03–0.756	51.0	55.3	54.5	48.0	50.6	28.2	47.5
0.03–0.796	50.2	54.7	54.3	47.2	50.0	26.2	47.5
0.03–0.856	50.0	55.3	54.7	46.9	50.1	24.5	47.9
average (%)		55.3	54.1		50.7		48.4

we estimated the temperature dependence from density measurements on the basis of the assumption that when the specimens with their maximum crystallinity by preheat-treatments were annealed again for 1 h at a constant temperature and were quenched immediately in ice water, the crystallinity of the quenched specimen is equal to that of the specimen at the constant temperature. As the crude results, it was confirmed that the crystallinity slightly decreases with the temperature. These results also support the ^{13}C NMR and X-ray diffraction results.

In this paper, the estimation of the morphology and the molecular mobility by ^{13}C solid-state NMR has been done without considering the NOE factor, but such a simple analysis contains serious problems as pointed by Schmidt-Rohr and Spiess.[33] This important contribution must be taken into account in further studies.

Conclusion

The characteristic phase structure of several types of polyethylene films such as melt films, single-crystal mats, undrawn dried gel films, and ultradrawn gel films was estimated by ^{13}C solid-state NMR. For all the specimens, the semilogarithmic plot of the ^{13}C magnetization of the peak height of the line at 33 ppm indicates that the overall decay curve can be classified into three components, a slow decay curve, a middle slow decay curve, and a rapid decay curve. Three T_{1C} values obtained from the initial slope of each curve indicated that the molecular mobility becomes more pronounced with increasing temperature, and this tendency was especially significant for specimens such as G201 with a low crystallinity at room temperature. Molecular packing in the orthorhombic crystal unit for the ultradrawn polyethylene with $\lambda = 300$ is thought to be more perfect than that for single-crystal mats, if the T_{1C} value reflects the molecular mobility directly. The T_{2C} value provided the information that for all the specimens, the noncrystalline component can be classified into two components which are associated with the interfacial region and rubber-like amorphous region with active molecular mobility. This is not in contradiction with the concept of Kitamaru and Horii.[19,22,23] Of course, the molecular mobility in both regions became more pronounced with temperature. The DD ^{13}C spectrum indicate that the crystallinity essentially decreases with temperature, and this tendency was in good agreement with the results measured by X-ray diffraction using Ruland's method. As for single-crystal mats and undrawn dried gel films, the mass fraction of the interfacial region was estimated by ^{13}C NMR, and the results were also in good agreement with the results by small-angle X-ray scattering on the basis of the concept that the boundary region corresponding to folded loops can be estimated from the plot of $\ln(Is^2)$ vs s^2.[30,31]

Acknowledgment. We are indebted to Prof. F. Horii, Chemical Research Institute, Kyoto University, for valuable comments on the ^{13}C NMR measurements and the analysis of the results. We also thank Drs. Deguchi and Sugisawa of the Japanese Electric Co. Ltd. We wish to express our thanks to Dr. D. L. VanderHart, National Institute of Standards and Technology, for valuable comments and suggestions for the analysis of the results.

References and Notes

(1) Smith, P.; Lemstra, P. J.; Kalb, B.; Pennings, A. J. *Polym. Bull.* **1979**, *1*, 733.
(2) Smith, P.; Lemstra, P. J.; Booij, H. C. *J. Polym. Sci., Polym. Phys. Ed.* **1979**, *19*, 877.
(3) Smith, P.; Lemstra, P. J. *J. Mater. Sci.* **1980**, *15*, 505.
(4) Smith, P.; Lemstra, P. J.; Pipper, J. P. L.; Kiel, A. M. *Colloid Polym. Sci.* **1980**, *258*, 1070.
(5) Matsuo, M.; Inoue, K.; Abumiya, N. *Sen-i-Gakkaishi* **1984**, *40*, 275.
(6) Furuhata, K.; Yokokawa, T.; Miyasaka, K. *J. Polym. Sci., Polym. Phys. Ed.* **1984**, *22*, 133.
(7) Matsuo, M.; Sawatari, C. Iida, M.; Yoneda, M. *Polym. J.* **1985**, *17*, 1197.
(8) Matsuo, M.; Sawatari, C. *Macromolecules* **1986**, *19*, 2653.
(9) Matsuo, M.; Sawatari, C.; Nakano, T. *Polym. J.* **1986**, *18*, 759.
(10) Sawatari, C.; Matsuo, M. *Macromolecules* **1989**, *22*, 2968.
(11) Ando, I.; Sorita, T; Yamanobe, T.; Komoto, T.; Sato, H.; Deguchi, K.; Imanari, M. *Polymer* **1985**, *26*, 1864.
(12) Ando, I.; Yamanobe, T.; Sorita, T.; Komoto, T.; Sato, H.; Deguchi, K.; Imanari, M. *Macromolecules* **1984**, *17*, 1955.
(13) Earl, W. L.; VanderHart, D. L. *Macromolecules* **1979**, *12*, 762.
(14) Vanderhart, D. L.; Khoury, F. *Polymer* **1984**, *25*, 1589.
(15) VanderHart, D. L. *J. Chem. Phys.* **1976**, *64*, 830.
(16) Opella, S. J.; Waugh, J. S. *J. Chem. Phys.* **1977**, *66*, 4919.
(17) Hama, T.; Suzuki, T.; Kosaka, K. *Kobunshi Ronbunshu* **1975**, *32*, 91.
(18) VanderHart, D. L.; Perez., E. *Macromolecules* **1986**, *19*, 1902.
(19) Kitamaru, R.; Horii, F.; Murauyama, K. *Macromolecules* **1986**, *19*, 636.
(20) Sozzani, P.; Simonutti, R.; Galimberti, M. *Macromolecules* **1993**, *26*, 5782.
(21) Matsuo, M.; Sawatari, C. *Macromolecules* **1988**, *21*, 1658.
(22) Nakagawa, M.; Horii, F.; Kitamaru, R. *Polymer* **1990**, *31*, 323.
(23) Zhu, Q.; Horii, F.; Tsuji, M.; Kitamaru, R. *Nihon Reoroji-Gakkaishi* **1989**, *17*, 35.
(24) Ogita, T.; Kawashara, Y.; Nakamura, R.; Ochi, T.; Minaagawa, M.; Matsuo, M. *Macromolecules* **1993**, *26*, 4646.
(25) Torchia, D. A. *J. Magn. Reson.* **1978**, *36*, 91.
(26) Hoseman, R.; Baguchi, S. N. *Direct Analysis of Diffraction by Matter*; North-Holland: Amsterdam, 1962.
(27) Blundell, D. J. *Acta Crystallogr.* **1970**, *A26*, 472.
(28) Matsuo, M.; Sawatari, C.; Tsuji, M.; Manley, R. St. J. *J. Chem. Soc., Faraday Trans. 2* **1983**, *79*, 1593.
(29) Matsuo, M.; Kitayama, C. *Polym. J.* **1985**, *17*, 479.
(30) Hashimoto, T.; Shibayama, M.; Kawai, H. *Macromolecules* **1980**, *13*, 1237.
(31) Sawatari, C.; Okumura, T.; Matsuo, M. *Polym. J.* **1986**, *18*, 741.
(32) Porod, G. *Kolloid Z. Z. Polym.* **1956**, *124* (2), 83; **1952**, *125* (1) 51; **1952**, *125* (2), 108.
(33) Schmidt-Rohr, K.; Spiess, H. W. *Macromolecules* **1991**, *24*, 5288.
(34) Axelson, D. E.; Mandelkern, L.; Popli, R.; Mathieu, P. *J. Polym. Sci., Polym. Phys. Ed.* **1983**, *21*, 2319.
(35) Kitamaru, R.; Horii, F.; Hyon, R. St. J. *J. Polym. Sci., Polym. Phys. Ed.* **1977**, *15*, 821.
(36) Kitamaru, R.; Horii, F. *Adv. Polym. Sci.* **1978**, *26*, 137.
(37) Matsuo, M.; Manley, R. St. J. *Macromolecules* **1982**, *15*, 985.
(38) Hentschel, D.; Sillescu, H.; Spiess, H. W. *Makromol. Chem.* **1970**, *180*, 241.
(39) McBrierty, V. J.; McDonald, I. R. *Polymer* **1975**, *16*, 125.
(40) Raff, R. A. V. In *Encyclopedia of Polymer Science and Technology*; Mark, H. F., et al., Eds.; Wiley: New York, 1967; Vol. 6, pp 275–332.
(41) Ruland, W. *Acta Crystallogr.* **1960**, *13*, 1059.
(42) Ruland, W. *Acta Crystallogr.* **1961**, *14*, 1180.
(43) Ruland, W. *Polymer* **1964**, *5*, 89.
(44) Killian, H. G. *Kolloid Z. Z. Polym.* **1962**, *183* 1; **1962**, *185*, 13.

MA946379P